Progress In Electromagnetics Research C, Vol. 76, 55–62, 2017

High Impedance Properties of Two-Dimensional Composite Right/Left-Handed Transmission Lines

Eiichi Sano[1] and Masayuki Ikebe[2, *]

Abstract—The electromagnetic characteristics of two-dimensional composite right/left-handed transmission lines (2D CRLH TLs) were investigated for the normal incidence of plane waves. The measured characteristic impedance and reflection phases exhibited resonant high impedance properties (equivalent to zero reflection phase) at a frequency within the left-handed mode for one-dimensional CRLH TL. An equivalent circuit was proposed to explain the measured characteristics. The relationship between the resonant frequency and the circuit parameters for 2D CRLH TLs was clarified by deriving an approximate equation for the resonant frequency.

1. INTRODUCTION

Metal wires in a three-dimensional cubic lattice and split ring resonators were respectively proposed to achieve negative permittivity and permeability [1, 2]. Left-handed metamaterials with simultaneously negative permittivity and permeability were produced [3, 4] by combining these concepts. However, these metamaterials are bulky three-dimensional structures and disadvantageous in use as microwave components. Thus, a composite right/left-handed transmission line (CRLH TL) was proposed to implement compact metamaterials on printed-circuit boards (PCBs) [5, 6]. Left-handed properties have been developed for electromagnetic waves propagating along one-dimensional (1D) CRLH TLs, and the design guidelines for CRLH TLs have been established on the basis of a simple equivalent circuit [5, 7]. CRLH TLs have been widely used to fabricate microwave components, such as directional couplers and leaky wave antennas [7, 8]. A two-dimensional configuration for the CRLH TLs (2D CRLH TLs) has also been investigated to understand their basic properties [5, 9, 10].

Another type of metamaterials, which has been widely used for antenna and electromagnetic compatibility (EMC) applications, is a high impedance surface (HIS) that was originally proposed with a so-called "mushroom structure" [11]. When plane waves are incident normally to the surface of the mushroom structure, the reflection phase is zero (high impedance) at the resonant frequency inherent to its structure. The mushroom structure has a frequency bandgap, in which no electromagnetic waves propagate along its surface. For this reason, the mushroom structure is also called an electromagnetic bandgap (EBG) structure. The sonant frequency rests on the EBG region in the mushroom structure, which is very useful as an antenna reflector to enhance antenna gain while preventing surface wave propagation.

The mushroom structure was investigated on the basis of 2D CRLH TL theory by Sanada et al. [9]. 2D CRLH TL theory was also used in the design of EBG-embedded microstrip patch antennas to enhance antenna gain [12]. Few investigations,on the other hand, have been reported on the electromagnetic behaviors of 2D CRLH TLs when plane waves are normally incident to their surfaces. Iwamoto et al. suggested that the mushroom structure was equivalent to 2D CRLH TLs for the normal incident

Received 9 May 2017, Accepted 13 July 2017, Scheduled 26 July 2017

* Corresponding author: Masayuki Ikebe (ikebe@ist.hokudai.ac.jp).

[1] Research Center for Integrated Quantum Electronics, Hokkaido University, Sapporo 060-8628, Japan. [2] Graduate School of Information Science and Technology, Hokkaido University, Sapporo 060-0814, Japan.

of plane waves [13]. However, the relationship between the reflection characteristics and the circuit parameters in an equivalent circuit of 2D CRLH TLs is still unclear. When 2D CRLH TLs are used as antenna reflectors similarly to those in the EBG structure, the resonant frequency needs to be situated in the bandgap between the left-handed (LH) and right-handed (RH) propagation modes of the 2D CRLH TLs to prevent surface wave propagation. Thus, it is important to clarify the relationship between resonant frequency and the bandgap for 2D CRLH TLs from both fundamental and practical aspects.

We investigated the electromagnetic characteristics of 2D CRLH TLs in this study for the normal incidence of plane waves on the basis of equivalent circuit analysis. Section 2 describes the experimental method, and Section 3 presents the measured and calculated characteristics for 1D and 2D CRLH TLs. Section 4 discusses the relationship between the reflection phase characteristics and circuit parameters for 2D CRLH TLs.

2. EXPERIMENTAL METHOD

Figure 1(a) is a photograph of part of a fabricated 2D CRLH TL and Figure 1(b) outlines an equivalent circuit for a 1D CRLH TL. Its substrate was FR4 with a thickness, t, of 1.6 mm and it had a metalized back side (ground plane). The right-handed (RH) components (L_R and C_R) were mainly produced by using a microstrip line (MSL). The left-handed (LH) components, L_L and C_L, were respectively produced by using a metalized via to ground and an interdigitated capacitor. The parasitic inductance in the interdigitated capacitor was added to L_R and the parasitic capacitance was added to C_R. The component values were calculated with the design equations described in Rahman and Stuchly [14] and Gupta et al. [15], which are summarized in the Appendix. The MSL width in the design of 2D CRLH TLs was first determined to be 3.2 mm so that the characteristic impedance of the MSL was $\sim 50\,\Omega$. Then, the length of the MSL and the geometry (size and the number of fingers) of the interdigitated capacitor were determined by assuming the diameter of the via hole was 0.3 mm, so that the bandgap between the LH and RH propagation modes in the 1D CRLH TL calculated with the design equations described by Caloz et al. [7] appeared at ~ 4 GHz to simplify the measurements. The design values of the components were: $L_R = 4.1$ nH, $C_R = 1.2$ pF, $L_L = 0.77$ nH, and $C_L = 0.5$ pF. The fabricated 2D CRLH TLs had 13×16 unit cells, where the unit cell length, p, was 12.8 mm.

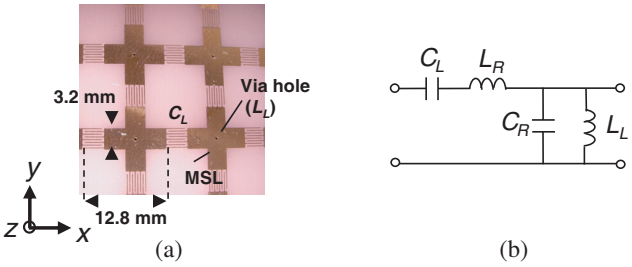

Figure 1. (a) Photograph of part of fabricated 2D CRLH TLs and (b) equivalent circuit for 1D CRLH.

A vector network analyzer (Keysight Technologies, E8361C) and a pair of horn antennas (Schwarzbeck, BBHA9120C) were used to measure the scattering (S) parameters for plane wave incidence. The two-port system was calibrated using the gated reflect line calibration method (Keysight Technologies, 85071E) [16]. The electric field of the incident plane wave was in the x-direction and the wave vector was in the z-direction. The S parameters for a 1D CRLH TL with the same geometry as 2D CRLH TLs were also measured with the vector network analyzer. The methods of extracting the characteristic impedance of the fabricated 2D CRLH TLs and the dispersion characteristics of the fabricated 1D CRLH TL from measured S parameters are summarized in the Appendix.

3. MEASURED AND CALCULATED RESULTS

The dispersion characteristics of the fabricated 1D CRLH TL were calculated from the measured S parameters for a 1D CRLH TL with nine cells. The measured and calculated dispersion characteristics

are compared in Fig. 2, where the parameter values used in the calculation were: $L_R = 3.8\,\text{nH}$, $C_R = 1.6\,\text{pF}$, $L_L = 0.77\,\text{nH}$, and $C_L = 0.5\,\text{pF}$. These values were determined by trial and error to fit the calculations to the measurements. Although L_R and C_R were slightly different from the designed values, good agreement was obtained between the measured and calculated dispersion characteristics. An LH propagation mode appeared in a frequency range from 2.6 to 3.6 GHz, while an RH propagation mode appeared in a frequency range from 4.7 to 6.7 GHz.

Figure 3 plots the imaginary part of measured characteristic impedance and the reflection phase of 2D CRLH TLs when plane waves are incident normally to the surface. Clear resonance was observed at 3.45 GHz, when the high impedance property (zero reflection phase) [11] emerged.

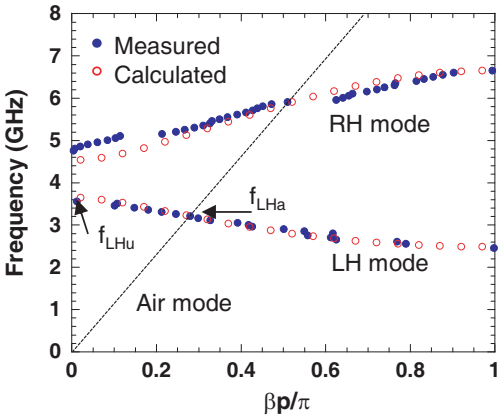

Figure 2. Comparison of measured and calculated dispersion characteristics for 1D CRLH TL.

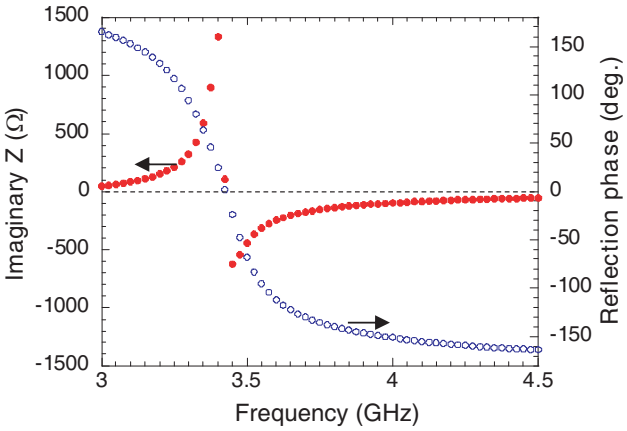

Figure 3. Measured characteristic impedance and reflection phase of 2D CRLH TLs for plane wave incidence.

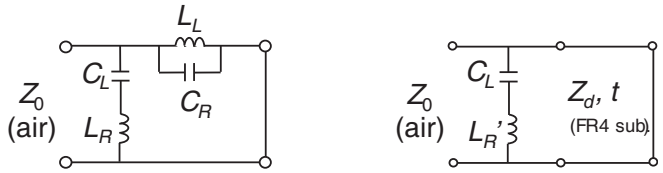

Figure 4. Candidate equivalent circuits of 2D CRLH TLs for plane wave incidence.

Two types of candidate equivalent circuits to explain the measured results are outlined in Fig. 4. We derived the equivalent circuit in Fig. 4(a) by changing the input and output ports for the 1D CRLH TL in Fig. 1(b). This equivalent circuit was first examined as to whether it explained the measured results. The characteristic impedance of the equivalent circuit is given by:

$$Z = \frac{(1-\omega^2 C_L L_R) j\omega L_L}{1-\omega^2(C_R L_L + C_L L_R + C_L L_L) + \omega^4 C_R C_L L_R L_L}. \tag{1}$$

The resonant frequencies are calculated as:

$$f_R = \frac{1}{2\pi}\sqrt{\frac{C_R L_L + C_L L_R + C_L L_L \pm \sqrt{(C_R L_L + C_L L_R + C_L L_L)^2 - 4C_R C_L L_R L_L}}{2C_R C_L L_R L_L}}. \tag{2}$$

The parameter values used in calculating the dispersion characteristics of 1D CRLH TL led to two resonances at 3.1 and 5.3 GHz. However, no resonance was observed at 5.3 GHz (not shown in Fig. 3). The characteristic impedance and the resonant frequency for the circuit without the capacitance C_R in

Fig. 4(a) are respectively given by:

$$Z = \frac{(1-\omega^2 C_L L_R) j\omega L_L}{1-\omega^2 C_L (L_R + L_L)} \tag{3}$$

and

$$f_R = \frac{1}{2\pi}\sqrt{\frac{1}{C_L(L_R+L_L)}}. \tag{4}$$

The calculated imaginary part of Z and the reflection phase are plotted in Fig. 5, where the L_R value was changed to 3.5 nH to match the calculated resonant frequency with the one that was measured. The calculated phase transition was steeper than that measured in the experiments.

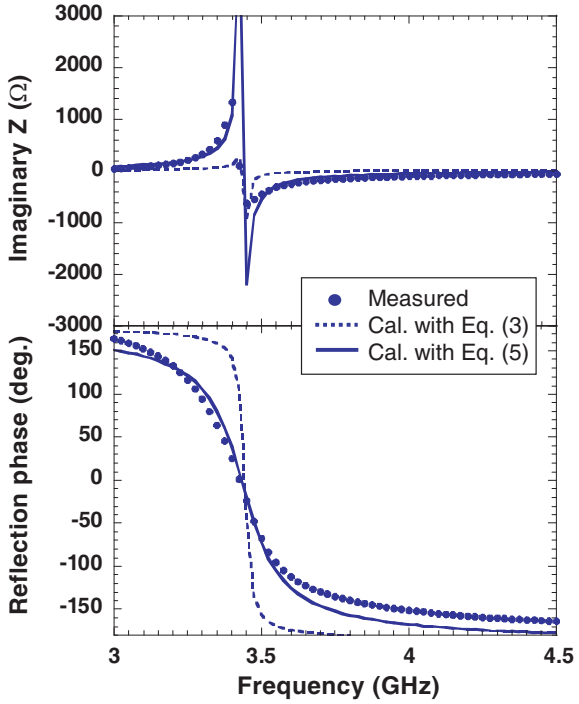

Figure 5. Comparison between measured and calculated characteristic impedance and reflection phases of 2D CRLH TLs for plane wave incidence.

The equivalent circuit outlined in Fig. 4(b) was advanced from the equivalent circuit for high impedance surfaces [17]. The FR4 substrate was modelled by a transmission line with a length of t (= substrate thickness) and characteristic impedance Z_d (= $Z_0/\varepsilon_d^{1/2}$, where Z_0 is the characteristic impedance of free space and ε_d is the relative permittivity of the substrate). Capacitance C_L was the same as the LH capacitance in the equivalent circuit of 1D CRLH TL, while inductance L'_R differed from the RH inductance, L_R. The difference was due to the difference in the direction of the electromagnetic field propagations for the 1D CRLH TL and the plane wave incident to the 2D CRLH TLs. The inductance value of L'_R was calculated with the design equations for metal strip inductance described in Gupta et al. [15].

A straight forward calculation led to the characteristic impedance of 2D CRLH TLs given by:

$$Z = \frac{j Z_d \tan(\beta t)}{1-\omega C_L Z_d \tan(\beta t)/(1-\omega^2 C_L L'_R)}, \tag{5}$$

where β is the wave number in the substrate. The calculated imaginary part of Z and reflection phase are plotted in Fig. 5. The inductance value of L'_R calculated with the design equations for metal strip

inductance described in Gupta et al. [15] was 2.07 nH, which was slightly different from the value of 2.25 nH that was determined to match the calculated resonant frequency with the measured one and used in the calculations in Fig. 5. Fairly good agreement was obtained between the measured and calculated results. The equivalent circuit in Fig. 4(b) more clearly explains the measured results than those in Fig. 4(a).

4. DISCUSSION

Iwamoto et al. treated a mushroom structure as 2D CRLH TLs and demonstrated that the resonant frequency was close to the Γ ($\beta = 0$) point in the dispersion curve for balanced 2D CRLH TLs (without a bandgap between LH and RH modes) [13]. However, the 2D CRLH TLs measured here had a bandgap between LH and RH modes, and the resonant frequency fell within the frequency region of the LH mode of the 1D CRLH TL. The resonant frequency was obtained on the basis of the equivalent circuit by equating the denominator of Eq. (5) to zero. Assuming $\tan(\beta t) \sim \beta t$, the resonant frequency is given by:

$$f_R = \frac{1}{2\pi}\sqrt{\frac{1}{C_L(L'_R + \mu_0 t)}}, \tag{6}$$

where μ_0 is the permeability of a vacuum. The upper bound frequency of the LH mode, f_{LHu}, denoted in Fig. 2 is given by Caloz et al. [7]:

$$f_{LHu} = \frac{1}{2\pi}\sqrt{\frac{1}{C_L L_R}}. \tag{7}$$

The $L'_R + \mu_0 t$ ($= 2.25 + 2.0$ nH) was larger than L_R ($= 3.8$ nH) in our case, which resulted in $f_{LHu} > f_R$. These results suggested that the resonant frequency was related to the upper bound frequency of the LH mode through the geometry of the metal strip in the TL. It was difficult to derive a simple expression that was related to these frequencies.

The dispersion characteristics for 2D CRLH TLs are different from their 1D counterparts [10]. The LH mode of a 1D CRLH TL in the fast wave region above the air mode (where the phase velocity of the LH mode was larger than the speed of light) was coupled to the air mode for 2D CRLH TLs. Note that the coupling was not included in the present equivalent circuit analysis. In addition, a surface transverse magnetic mode appeared between the bandgap between the LH and RH modes of a 1D CRLH TL, which followed the air mode [10]. The LH mode of the 1D CRLH TL intersected the air mode at 3.22 GHz, which is indicated as f_{LHa} in Fig. 2. Since the LH mode was coupled to the air mode, the upper bound frequency of the LH mode in the 2D CRLH TLs became lower than the intersection frequency, f_{LHa}.

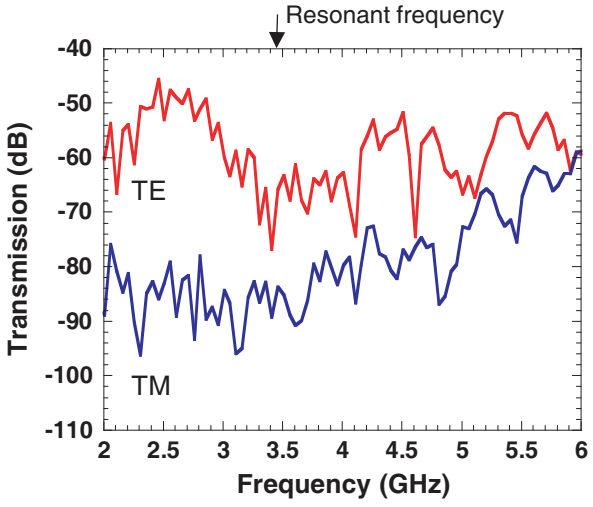

Figure 6. Surface mode transmission characteristics for 2D CRLH TLs.

This suggested that the resonant frequency, f_R, was situated in the bandgap of the 2D CRLH TLs that were used here. The transverse magnetic (TM) and transverse electric (TE) surface modes for the fabricated 2D CRLH TLs were measured to investigate the effect of the air mode by using small coaxial probes similar to those described in Sievenpiper et al. [11]. The results obtained from measurements are plotted in Fig. 6. The transmission band from 2.4 to 3.0 GHz was narrower than the frequency region for the LH mode of the 1D CRLH TL, which suggested coupling between the LH and air modes. The transmission at the resonant frequency indicated by the arrow in Fig. 6 was ~ 15 dB lower than that in the 2.4–3.0 GHz band. This supported the hypothesis that resonant frequency f_R was situated in the bandgap of the 2D CRLH TLs used here.

5. CONCLUSION

We measured the S parameters of the fabricated 2D CRLH TLs for the normal incidence of plane waves. A clear resonance was observed at 3.45 GHz, when a high impedance property (zero reflection phase) emerged. Equivalent circuit analysis matched the measured impedance and reflection phase characteristics. The relationship between the resonant frequency and the circuit parameters for 2D CRLH TLs was clarified by deriving an approximate equation for the resonant frequency. The measured surface-wave transmission characteristics for the 2D CRLH TLs indicated that the resonant frequency was situated in the bandgap of the 2D CRLH TLs. Although the configurations for 2D CRLH TLs were more complicated than the mushroom structure, the flexibility of design for the properties of high impedance surfaces, such as operation frequency, may be expanded by using commercially available chip components for the LH and RH components in 2D CRLH TLs from the simple mushroom structure.

APPENDIX A. DESIGN EQUATIONS FOR CALCULATING COMPONENT VALUES

Capacitance C in an RH TL with a unit length (1 m) are given by Gupta et al. [15] as:

$$C = \begin{cases} 2\pi\varepsilon_0\varepsilon_{re}/\ln(8t/W + 0.25W/t) & (W/t \le 1) \\ \varepsilon_0\varepsilon_{re}\left[W/t + 1.393 + 0.667\ln(W/t + 1.444)\right] & (W/t \ge 1) \end{cases}, \tag{A1}$$

where W is the width of the TL, t the substrate thickness, ε_0 the permittivity of a vacuum, and effective relative permittivity ε_{re} is given by

$$\varepsilon_{re} = \begin{cases} \dfrac{\varepsilon_d + 1}{2} + \dfrac{\varepsilon_d - 1}{2}\left[(1 + 12t/W)^{-1/2} + 0.04(1 - W/t)^2\right] & (W/t \le 1) \\ \dfrac{\varepsilon_d + 1}{2} + \dfrac{\varepsilon_d - 1}{2}(1 + 12t/W)^{-1/2} & (W/t \ge 1) \end{cases}. \tag{A2}$$

Inductance L in an RH TL with a unit of length (1 m) are given by Gupta et al. [15] as:

$$L = \frac{1}{c^2 C_0}, \tag{A3}$$

where c is the speed of light and C_0 is calculated by replacing ε_{re} with one in (A1).

The capacitance in an interdigitated capacitor in a unit of pF is given by Gupta et al. [15] as:

$$C_L = \frac{\varepsilon_{re}}{18\pi}\frac{K(k)}{K(\sqrt{1 - k^2})}(n - 1)l, \tag{A4}$$

where K is the complete elliptic integral of the first kind, n the number of fingers, l the finger length in units of millimeters, and k is given by:

$$k = \tan^2\left(\frac{a\pi}{4b}\right) \tag{A5}$$

with

$$a = \frac{w}{2} \quad \text{and} \quad b = \frac{w + s}{2}, \tag{A6}$$

where w and s correspond to the finger width and space. The parasitic inductance and capacitance in the interdigitated capacitor are calculated by using Eqs. (A1)–(A3) by replacing W with w. The $w = 0.14$ mm and $s = 0.28$ mm in our CRLH TLs.

The inductance of a metalized via to the ground is given by Rahman and Stuchly [14] as:

$$L_L = 2 \times 10^{-7} t \left[\ln\left(\frac{4t}{d}\right) + 0.5\frac{d}{t} - 0.75 \right], \tag{A7}$$

where d is the diameter of the via. The $d = 0.3$ mm in our CRLH TLs.

APPENDIX B. METHODS OF EXTRACTING CHARACTERISTIC IMPEDANCE AND DISPERSION CHARACTERISTICS FROM MEASURED S PARAMETERS

The characteristic impedance of the 2D CRLH TLs was calculated from the S parameters measured for plane wave incidence by using [3]:

$$Z = Z_0 \frac{1 + S_{11}}{1 - S_{11}}. \tag{B1}$$

The propagation constant, $\gamma(= \alpha + j\beta)$, for the 1D CRLH TL with nine cells was obtained by solving:

$$e^{2\gamma p_9} - (A + D)e^{\gamma p_9} + AD - BC = 0, \tag{B2}$$

where p_9 is the length of nine cells, and A, B, C, and D are the components of the $ABCD$ matrix converted from the measured S parameters. The product of the propagation constant and length for the unit cell of the 1D CRLH TL, γp, was calculated by dividing γp_9 by nine, and the imaginary part of γp was equal to βp (the lateral axis) in Fig. 2.

REFERENCES

1. Pendry, J. B., A. J. Holden, W. J. Stewart, and I. Youngs, "Extremely low frequency plasmons in metallic mesostructures," *Physical Review Letters*, Vol. 76, No. 25, 4773–4776, 1996.
2. Pendry, J. B., A. J. Holden, D. J. Robbins, and W. J. Stewart, "Magnetism from conductors and enhanced nonlinear phenomena," *IEEE Transactions on Microwave Theory and Technology*, Vol. 47, No. 11, 2075–2084, 1999.
3. Smith, D. R., W. J. Padilla, D. C. Vier, S. C. Nemat-Nasser, and S. Schultz, "Composite medium with simultaneously negative permeability and permittivity," *Physical Review Letters*, Vol. 84, No. 18, 4184–4187, 2000.
4. Shelby, R. A., D. R. Smith, and S. Schultz, "Experimental verificationof a negative index of refraction," *Science*, Vol. 292, 77–79, 2001.
5. Eleftheriades, G. V., A. K. Iyer, and P. C. Kremer, "Planar negative refractive index media using periodically L-C loaded transmission lines," *IEEE Transactions on Microwave Theory and Technology*, Vol. 50, No. 12, 2702–2712, 2002.
6. Liu, L., C. Caloz, and T. Itoh, "Dominant mode leaky-wave antenna with backfire-to-endfire scanning capability," *Electronics Letters*, Vol. 38, No. 23, 1414–1416, 2002.
7. Caloz, C., A. Sanada, and T. Itoh, "A novel composite right-/left-handed coupled-line directional coupler with arbitrary coupling leveland broad bandwidth," *IEEE Transactions on Microwave Theory and Technology*, Vol. 52, No. 3, 980–992, 2004.
8. Lai, A., C. Caloz, and T. Itoh, "Composite right/left-handed transmission line metamaterials," *IEEE Microwave Magazine*, 34–50, Sep. 2004.
9. Sanada, A., C. Caloz, and T. Itoh, "Planar distributed structures with negative refractive index," *IEEE Transactions on Microwave Theory and Technology*, Vol. 52, No. 4, 1252–1263, 2004.
10. Kokkinos, T., C. D. Sarris, and G. V. Eleftheriades, "Periodic finite-difference time-domain analysis of loaded transmission-line negative-refractive-index metamaterials," *IEEE Transactions on Microwave Theory and Technology*, Vol. 53, No. 4, 1488–1495, 2005.
11. Sievenpiper, D., L. Zhang, R. F. Jimenez Broas, N. G. Alexopolous, and E. Yablonovitch, "High-impedance electromagnetic surfaces with a forbidden frequency band," *IEEE Transactions on Microwave Theory and Technology*, Vol. 47, No. 11, 2059–2074, 1999.

12. Chandrasekaran, K. T., M. F. Karim, Nasimuddin, and A. Alphones, "CRLH structure-based high-impedance surface for performance enhancement of planar antennas," *IET Microwaves, Antennas & Propagation*, Vol. 11, No. 6, 818–826, 2017.
13. Iwamoto, S., A. Sanada, and H. Kubo, "Experimental investigation of reflection characteristics of a high-impedance surface by 2D balanced CRLH metamaterials without a forbidden frequency band," *Proceedings of Asia-Pacific Microwave Conference*, 1–4, 2007.
14. Rahman, M. and M. A. Stuchly, "Transmission line-periodic circuit representation of planar microwave photonic bandgap structures," *Microwave and Optical Technology Letters*, Vol. 30, No. 1, 15–19, 2001.
15. Gupta, K. C., R. Garg, I. Bahl, and P. Bhartia, *Microstrip Lines and Slotlines*, 2nd Edition, Artech House, Norwood, MA, 1996.
16. http://www.keysight.com/upload/cmc_upload/All/FreeSpaceSeminarRev2.pdf.
17. Mosallaei, H. and K. Sarabandi, "Antenna miniaturization and bandwidth enhancement using a reactive impedance substrate," *IEEE Transactions on Antennas and Propagation*, Vol. 52, No. 9, 2403–2414, 2004.